



Preferential arrangement of lipids in the long-periodicity phase of a stratum corneum matrix model[§]

Charlotte M. Beddoes, Gert S. Gooris, and Joke A. Bouwstra¹

Leiden Academic Centre for Drug Research, Division of BioTherapeutics, Gorlaeus Laboratories, University of Leiden, Leiden, The Netherlands

Abstract The lipid matrix of the stratum corneum, the outermost skin layer, consists primarily of ceramides, cholesterol, and FFAs. These lipids form a trilayer long-periodicity phase (LPP) that is unique to this barrier. Knowledge about the LPP is essential in understanding the barrier function. Previous studies of LPP lipid models have identified the position of the major lipid classes and suggested that a large fraction of FFAs and the ceramide acyl chain are present in the central region. However, the precise arrangement, such as lipid subclass mixing (isolated or mixed) and ceramide conformation (extended or hairpin), remains unknown. Here, we deuterated FFAs and the ceramide acyl chain to study CD₂ and CH₂ interactions with Fourier-transform infrared spectroscopy. The ceramide and FFAs of various chain lengths were not in separate domains but had mixed together. The larger number of CD₂-CD₂ lipid chain interactions in the LPP than in a symmetrical bilayer structure implied that the ceramide had primarily adopted an extended conformation. Shorter FFAs were present in the central region of the LPP. This model explores the biophysical properties of the stratum corneum's LPP to improve the understanding of the barrier function of this layer.—Beddoes, C. M., G. S. Gooris, and J. A. Bouwstra. Preferential arrangement of lipids in the long-periodicity phase of a stratum corneum matrix model. *J. Lipid Res.* 2018. 59:2329–2338.

Supplementary key words skin • ceramide • fatty acids • membranes • physical chemistry • physical biochemistry • sphingolipids • Fourier-transform infrared spectroscopy • lipid conformation • partial deuteration

The skin's principal function as a controlled interface between the body and external environment is to impede substances from entering the body while preventing desiccation from within. The barrier is located in the outermost layer of the skin, the stratum corneum (SC). The SC consists of dead corneocytes encased in a lipid matrix that is often compared structurally with a brick wall (1). The lipid matrix is the only structure that extends entirely through the SC, and as a result understanding the skin's barrier is of great interest. The lipids can implement such an effective barrier due to their highly ordered crystalline lamellar

structures. The organization of these lipids are directly correlated to the barrier properties of the skin, which are evident by the alterations observed both in the composition and organization of the SC layer of diseased skin (2–8). Understanding the organization of these lipids enables improved insights into the differences between healthy and diseased SC.

The lipid matrix is primarily composed of ceramides (CERs), cholesterol (CHOL), and FFAs in a 1:1:1 molar ratio (9). The lipid subclass composition is highly complex and contains a wide range of different lipids. In the case of the CERs, 18 subclasses have been identified in human SC (10), and each of these subclasses have additionally shown a large variation in their carbon chain length. A large variation in FFA chain length is also present in the SC (11–13). X-ray diffraction studies have revealed that the SC lipids are arranged as two coexisting lamellar phases with repeat distances of approximately 13 and 6 nm, which are referred to as the long-periodicity phase (LPP) and short-periodicity phase (SPP), respectively (14). The LPP is unique to the skin barrier and is assumed to be an important factor in its barrier capability (15). In parallel, the lateral packing also affects the permeability of the skin. The lipids in the SC layer are primarily packed in an orthorhombic structure, with a smaller population forming a less densely packed hexagonal or liquid phase (16).

With the use of model systems, previous work has identified the relative positions of several of the lipid subclasses (17–19). CERs with a nonhydroxyl C24 acyl chain linked to a C18 sphingosine (NS) and FFAs were located in the central region of the LPP trilayer structure, while CHOL remained exclusively in the outer region (18). CER EOS is uniquely positioned in both the outer and interior regions, with the head groups present at the boundary of the unit cell, while the carbon chain extends to the central head

Abbreviations: CER, ceramide; CHOL, cholesterol; dFFA, perdeuterated FFA; FTIR, Fourier-transform infrared spectroscopy; LB, lamellar bilayer; LPP, long-periodicity phase; NS, sphingosine; SAXD, small-angle X-ray diffraction; SC, stratum corneum; SPP, short-periodicity phase.

¹To whom correspondence should be addressed.

e-mail: bouwstra@lacdr.leidenuniv.nl

[§]The online version of this article (available at <http://www.jlr.org>) contains a supplement.

Manuscript received 18 May 2018 and in revised form 28 September 2018.

Published, *JLR Papers in Press*, October 17, 2018

DOI <https://doi.org/10.1194/jlr.M087106>

Copyright © 2018 Beddoes et al. Published under exclusive license by The American Society for Biochemistry and Molecular Biology, Inc.

This article is available online at <http://www.jlr.org>

group region, where the linoleate moiety resides. This knowledge has enabled the construction of a lipid LPP model (S1). However, in the proposed LPP models it remains ambiguous how the lipid subclasses are arranged in their respective regions. In addition, the conformation of the CERs remains uncertain. The dual alkyl chains of the CERs can be arranged either as an extended lipid or back on themselves in a hairpin structure (Fig. 1).

In this study, we focused on the specific interactions between CER NS and FFA chains in the LPP unit cell using Fourier-transform infrared spectroscopy (FTIR) analysis by partial deuteration of these chains. A simple lipid model system consisting of two CERs, CHOL, and five FFAs that form the LPP exclusively was used to study whether these lipids mixed together or formed isolated domains in the LPP. These models were compared with a simple lamellar bilayer (LB) structure to determine whether the amount of carbon interactions between selectively deuterated lipids in the LPP is different from that of a normal bilayer system. We determined that between selected FFAs and CERs they would preferentially interact with one another in the LPP unit cell. In addition, these interactions identified the conformation of the CER NS and the location of shorter-chain FFAs in the LPP.

MATERIALS AND METHODS

Materials

The structures of the synthetic lipids used in this study are presented in Fig. 2. The synthetic CER EOS, with an acyl carbon chain length of 30, and NS (C24), with a deuterated fatty acid moiety (referred to as d47-NS), were provided by Evonik (Essen, Germany). Palmitic acid (C16), stearic acid (C18), arachidic acid (C20), behenic acid (C22), lignoceric acid (C24), CHOL, acetate buffer salts, and deuterated water were obtained from Sigma-Aldrich Chemie GmbH (Schnelldorf, Germany). The perdeuterated FFAs (dFFAs) with chain lengths of C18 and C20 were purchased from Cambridge Isotope Laboratories (Andover, MA). The dFFAs with chain lengths of C16 and C22 were obtained from Larodan (Malmö, Sweden). dFFA with a chain length of C24 was obtained from Arc Laboratories BV (Apeldoorn, the Netherlands). All solvents used were of analytical grade and supplied by Labscan (Dublin, Ireland). The water was produced by a Milli-Q water filtration system (Millipore, Burlington, MA) with a resistivity of 18 M Ω cm at 25°C.

Lipid model composition

The model lipid mixtures were prepared from synthetic CERs, CHOL, and FFAs in an equimolar ratio for the LPP system. The lipid ratios for the LB models are described in Table 1. The CER

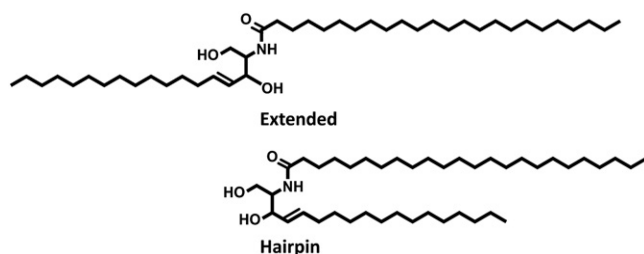


Fig. 1. Extended and hairpin conformations of CERs.

composition in the LPP model consisted of EOS and NS. CER NS was selected, with CER EOS, due to its capability to form the LPP. To ensure that the LPP was exclusively formed, the CER EOS level was set to 40 mol% of the total CER concentration (20, 21). The FFA composition was prepared from five FFA subclasses with carbon chain lengths of C16, C18, C20, C22, and C24 at molar ratios of 1.8, 4.0, 7.6, 47.8, and 38.8, respectively, a composition similar to SC (11).

Lipid model preparation

The appropriate amount of lipids was dissolved in a chloroform-methanol (2:1; v/v) solution at concentrations ≤ 5 mg/ml. Subsequently, 0.75 mg of lipids were sprayed on mica over an area of 0.2×0.5 cm² for the small-angle X-ray diffraction (SAXD) samples or 1.5 mg of lipids on AgBr windows over an area of 1×1 cm² for FTIR measurements. Samples were sprayed using a Camag Linomat IV sample applicator (Muttentz, Switzerland). Once sprayed, the samples were slowly heated to either 85°C for LPP samples, or 120°C for LB samples, to ensure the samples had melted. Samples were left at this temperature to equilibrate for 10 min, and then the samples were slowly cooled back to room temperature, after which the equilibration cycle was repeated. The sample was then subsequently hydrated in deuterated acetate buffer for FTIR measurements, or sodium bromide solution for X-ray measurements, at 100% relative humidity at 38°C for >15 h prior to measurement.

FTIR measurements

The FTIR setup consisted of a Frontier FT-IR spectrometer (PerkinElmer, Buckinghamshire, UK) equipped with a broad-band mercury cadmium telluride detector cooled with liquid nitrogen. The sample was purged continuously under dry air that started ≥ 10 min before the measurement and continued up to the end of the experiment. A spectrum at a given temperature was averaged between 77 individual measurements that were collected in absorbance mode at a resolution of 1 cm⁻¹ over 4 min. To measure the phase transition in relation to the temperature, the sample was heated at a rate of 0.25°C/min to measure a 1°C increase per recorded spectrum. The spectra were collected between 0 and 90°C using the Spectrum TimeBase software (PerkinElmer). The spectra were processed in Spectrum and plotted using in-house Enthought Canopy scripts. To accurately determine the peak position of the scissoring (δ) vibrations, the peaks were measured after calculating the second derivative. At least two samples were prepared and measured for each experimental condition.

SAXD measurements

SAXD measurements were taken at the European Synchrotron Radiation Facility. The wavelength was set at 1.033 Å, and the detector distance was fixed at 2.16 m. A Pilatus 1M detector was used; the sensor was a reverse-biased silicon-diode array consisting of 981×1043 pixels, 172×172 μm^2 in size. The calibration was performed using silver behenate. Samples were measured for 90 s at 25°C. The 1D intensity profiles were determined by integrating the 2D pattern along the Cartesian and polar coordinates with the scattering angle (θ). The scattering intensity (I) was measured as a function of the scattering vector q , which is proportional to θ and the wavelength λ of the X-ray beam and is calculated according to Bragg's law as follows:

$$q = \frac{4\pi \sin \theta}{\lambda} \quad (\text{Eq. 1})$$

When in the lamellar phase, a series of peaks at equal distances to one another are observed. The d-spacing (d_n) of the lamellar phase can be calculated as

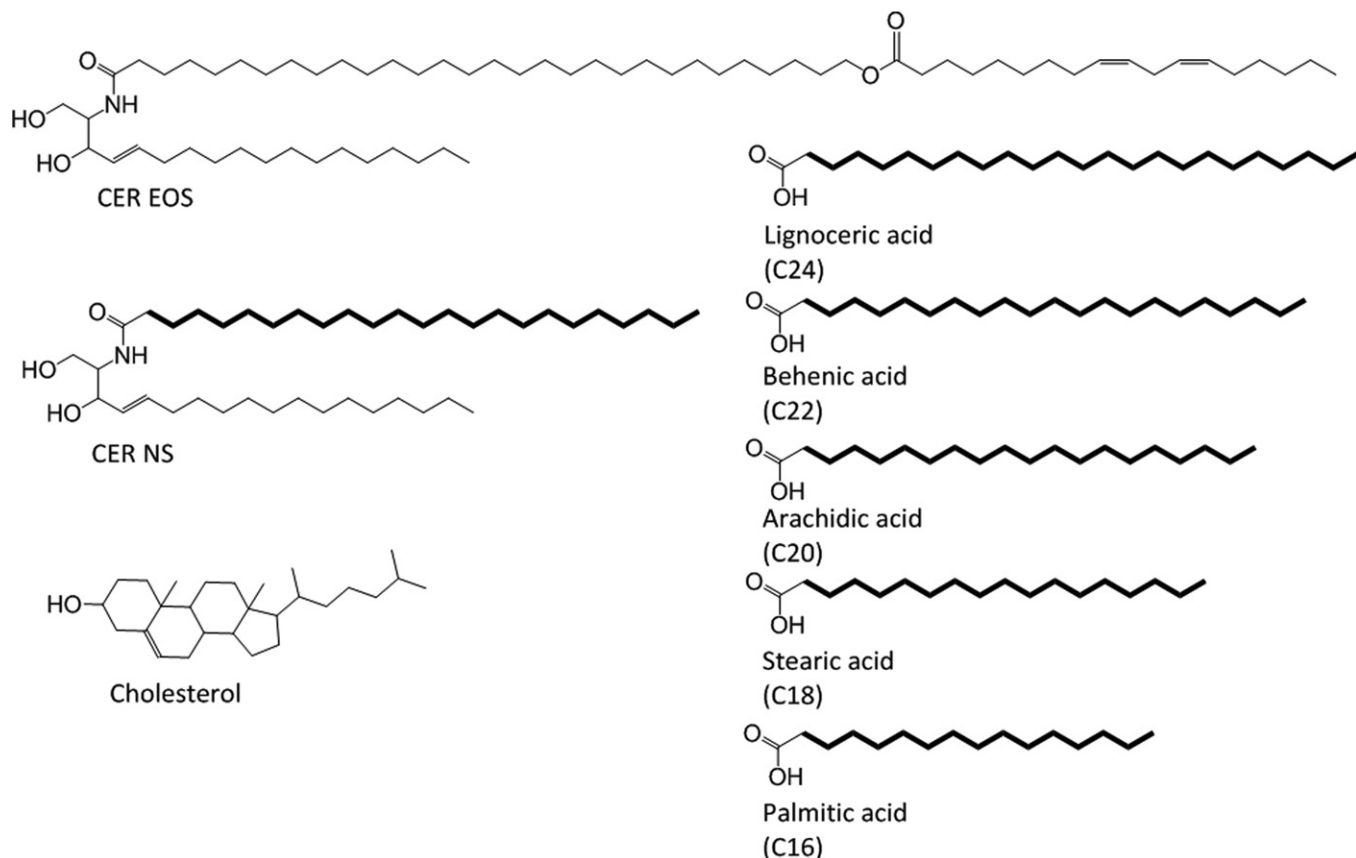


Fig. 2. The molecular structure of the lipids used in this investigation. The protiated lipids include CER EOS (C30), CER NS (C24), FFAs C16–C24, and CHOL. The deuterated moieties are highlighted in bold.

$$d_n = \frac{2n\pi}{q_n} \quad (\text{Eq. 2})$$

with n as the order number of the diffraction peak located at position q_n . Each sample was prepared and measured at least in duplicate.

RESULTS

The LPP model was measured with various deuterated lipid-component substitutions to enable isolated lipid acyl chain measurements to investigate the lipid interactions. The X-ray diffraction curve of the fully protiated synthetic LPP (LPP-CH₂) shows eight orders (**Fig. 3A**). The LPP has a periodicity of 12.9 nm. Similiar to native SC, a proportion of the CHOL in the sample had phase separated.

The thermotropic phase behavior was determined via both the δ and symmetric stretching (ν) vibrations of the lipid alkyl chains (**Fig. 3B, C**). In the δ region, the peak splitting occurred from the close proximity of neighboring highly organized lipid CH₂ alkyl chains, which enables short-range coupling interactions. It is these coupling interactions that induced the observed peak splitting. As the temperature increased, a transition from the orthorhombic to hexagonal phase was observed, as shown in the δ thermotropic response curve (**Fig. 3B**) and indicated by the formation of a single central peak at the expense of the two orthorhombic peaks. The single peak is a product of a small increase in the spacing between the lipid alkyl chains. The increase in the lipid spacing can occur when the lipids pack either in the hexagonal or fluid phase. The greater

TABLE 1. Sample composition used in this experiment

Sample Name	CER	FFAs
LPP-CH ₂	EOS/NS	C16/C18/C20/C22/C24
LPP-dNS	EOS/ d47-NS	C16/C18/C20/C22/C24
LPP-dFFAs	EOS/NS	d31-C16/d35-C18/d39-C20/d43-C22/d47-C24
LPP-dNS/dC24	EOS/ d47-NS	C16:0/C18:0/C20:0/C22:0/ d47-C24
LPP-dNS/dFFAs	EOS/ d47-NS	d31-C16/d35-C18/d39-C20/d43-C22/d47-C24
dFFA	—	d31-C16/d35-C18/d39-C20/d43-C22/d47-C24
LB-dNS/dC24 (6:4)	d47-NS	d47-C24
LB-dNS/dFFA (3:5)	d47-NS	d31-C16/d35-C18/d39-C20/d43-C22/d47-C24

The deuterated labeled lipids (d) are highlighted in bold. All LPP samples additionally contained CHOL in an equal molar ratio to CERs and FFAs, while the lipid ratios in the LB samples are expressed in the table.

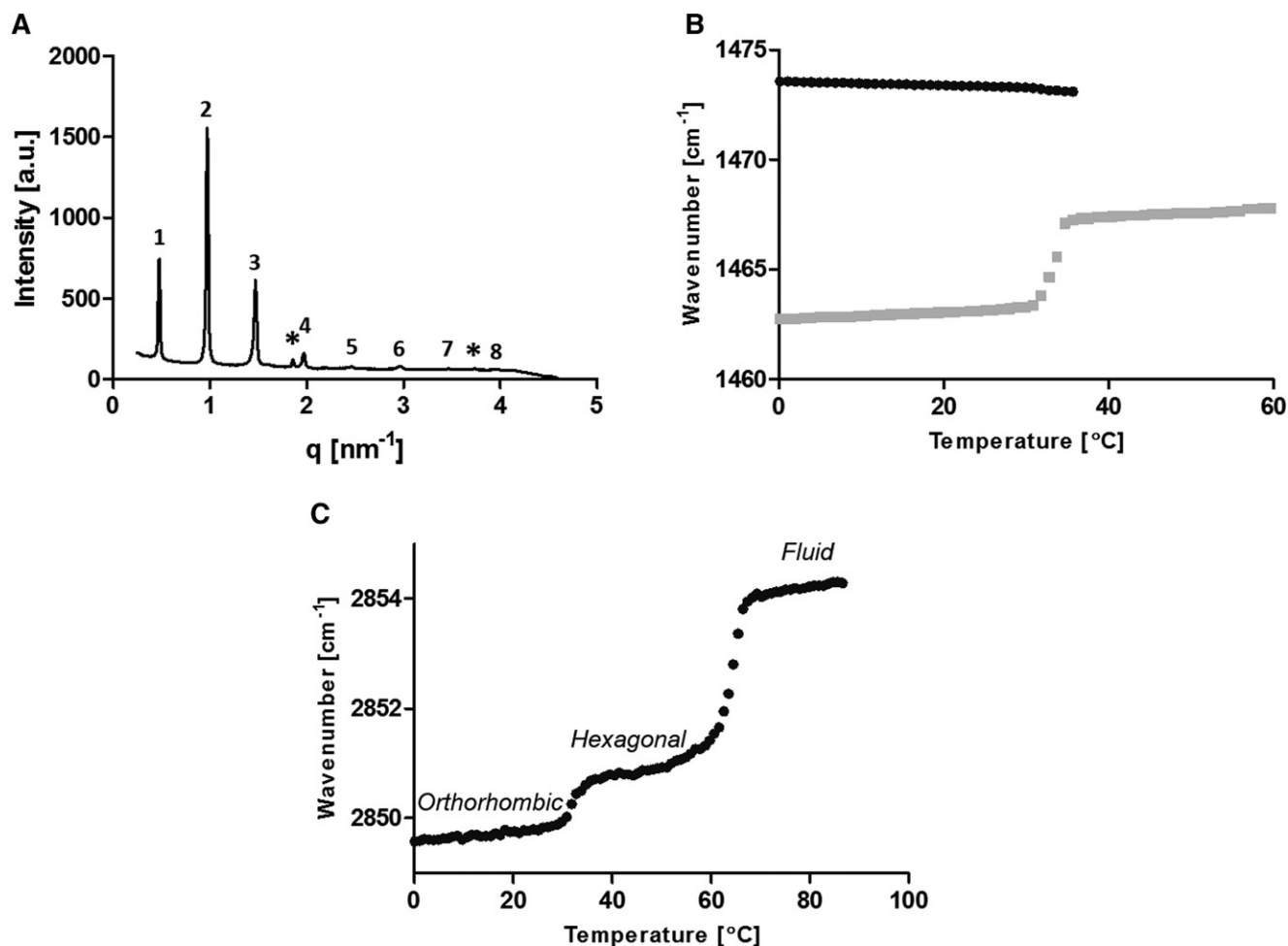


Fig. 3. LPP-CH₂ analysis. A: SAXD curve at 25°C. Both the LPP (numbered) at q values of 0.49, 0.97, 1.47, 1.97, 2.47, 2.97, 3.47, and 3.96 and CHOL single-crystal peaks (*) at q values of 1.86 and 3.74 nm⁻¹ are detected in the sample. B, C: Thermotropic analysis of the δ and ν vibrational energy from FTIR analysis, respectively, highlighting the lateral phase transition temperatures by the loss of the peak split or an increase in the peak's wavenumber.

lipid distances prevent the lipids' acyl chain from coupling with their neighbors, which prevents the peak splitting effect. In the thermotropic response curve of the ν region (Fig. 3C), the orthorhombic to hexagonal phase transition temperatures are observed by a slight increase in the peak wavenumber, which occurs at temperatures between 34 and 40°C. In contrast, the hexagonal to fluid phase transition is observed at temperatures between 60 and 69°C. The greater wavenumber increase during this phase transition indicated a larger amount of disorder in the lipid chains (ordered to a liquid-state transition).

To focus on the alkyl chain interactions suspected to be present in the central region of the LPP (S1), the acyl chain of CER NS and/or FFAs was selectively deuterated in a series of four samples to investigate their interactions (Table 1). To determine the degree of integration of the deuterated lipids with the protiated lipids, the chain melting behavior was observed by their ν vibrations with FTIR (Fig. 4). The phase transition temperatures for all four partially deuterated samples in the LPP did not deviate from the fully protiated sample (Fig. 3C). In addition, both the protiated and deuterated components of each sample melted to form the liquid phase at the same temperature

range as the fully protiated sample (60–69°C); thus, the deuterated lipid substitution in the LPP samples did not indicate that phase-separated domains were present, and instead the partially deuterated lipids remained integrated with the protiated lipids.

In the orthorhombic phase, when a sample is partially deuterated, the δ vibrations of the CH₂ and CD₂ alkyl chains cannot interact due to their large vibrational energy difference (CH₂: $\sim 1,470$ cm⁻¹; CD₂: $\sim 1,090$ cm⁻¹). Thus, if these lipids were neighboring one another, the observed peak splitting would be lost. As a result, the width of the peak splitting is proportional to the same isotopic chain domain size (23–25). In terms of the samples, with the addition of partially deuterated material in the orthorhombic phase, a single δ peak indicates that the isotopic equivalent chains had not exclusively aggregated together but instead mixed with the protiated lipid chains (22).

The δ peak splitting was examined at 1°C to ensure the maximum amount of lipids were packed in the orthorhombic phase. The CER dNS interactions in the LPP-dNS sample are shown in Fig. 5A. The sharp single CD₂ peak observed demonstrates that the CER NS CD₂ acyl chains were unable to interact with other neighboring CD₂ CER

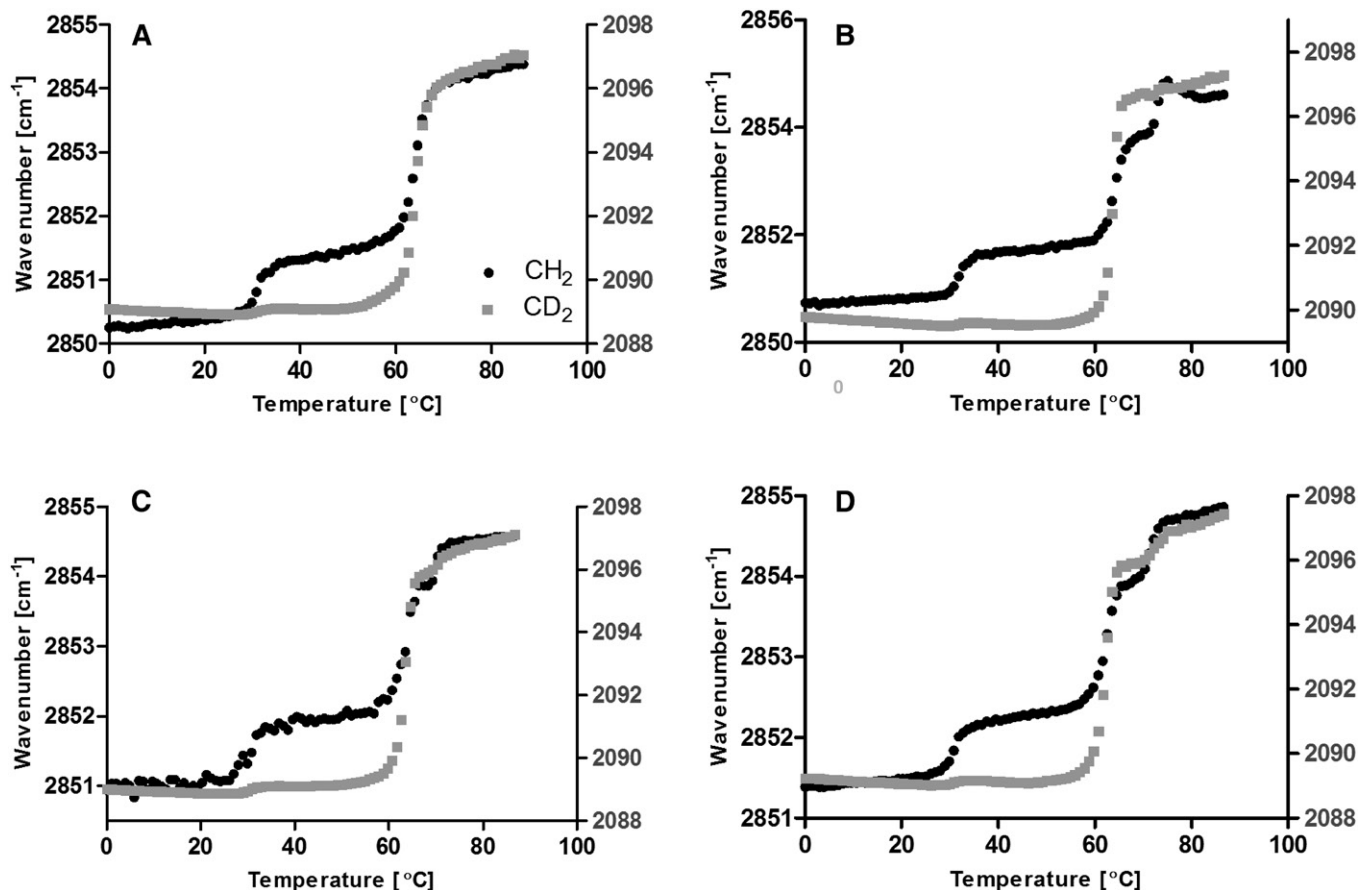


Fig. 4. Thermotropic ν vibration curves for LPP-dNS (A), LPP-dFFAs (B), LPP-dNS/dC24 (C), and LPP-dNS/dFFAs (D). Both the CH_2 (black circle) and CD_2 (gray square) lipids melted over the same temperature range, implying that the deuterated lipids were integrated with the protiated lipids in the LPP.

NS alkyl chains, implying that the CD_2 chain was in a CH_2 -rich environment. Thus, it can be concluded that the deuterated acyl chain of CER NS was dispersed from one another in the LPP and did not form isolated domains.

Figure 5B shows the δ CH_2 vibrations of the remaining protiated alkyl chains for the LPP-dNS sample. The lipids that remained protiated included the CER EOS, CER NS sphingosine moiety, CHOL, and FFAs. Due to the large number of protiated alkyl chains in the sample, they could interact, resulting in a peak splitting of 9.1 cm^{-1} . This splitting was narrower compared with the fully protiated sample peak split of 10.8 cm^{-1} (Table 2, Fig. 6A). In addition, the shape of the doublet also changed. Figure 6A shows the splitting curve of the LPP- CH_2 sample when the lipids were in the orthorhombic phase. In contrast, the CH_2 splitting observed in LPP-dNS showed a shallower minima between the split peaks, signifying that CH_2 - CD_2 interactions were present. These results confirm that the deuterated acyl chains of CER NS partly disrupted CH_2 interactions by mixing with the protiated chains in the LPP.

When the FFAs were deuterated (LPP-dFFAs), the CD_2 δ peak was broader (Fig. 5A) compared with the LPP-dNS sample, which indicated a larger number of CD_2 - CD_2 chain interactions. The increase in the peak width was small, and no peak splitting was observed, implying a large proportion of the CD_2 chains also interacted with CH_2 lipids,

thus signifying FFAs were also mixed with the other protiated lipids within the sample. The LPP-dFFAs CH_2 splitting (Fig. 5B) formed a plateaued maximum. This was due to the higher relative intensity of the CH_2 - CD_2 central peak. The width of the peak splitting decreased compared with LPP-dNS (6.2 and 9.1 cm^{-1} , respectively), which showed a greater proportion of mixed isotope interactions were present in the LPP-dFFAs sample compared with the LPP-dNS sample. As such, this demonstrates that the FFAs were not aggregated into isolated lipid domains in the LPP.

In the LPP-dNS/dC24 sample, both the CER NS acyl chain and FFA C24 acyl chains were deuterated. These chains showed a visible CD_2 peak split with a splitting width of 4.6 cm^{-1} . This peak was wider compared with the LPP-dNS and LPP-dFFA (Fig. 5A). The formation of a split peak implied there was an increase in the CD_2 - CD_2 interaction ratio, equating to a larger CD_2 domain, at the expense of CD_2 - CH_2 interactions. The deuteration molar percentage in both LPP-dNS/dC24 and LPP-dFFA samples was similar (32.9% and 33.3% , respectively); thus, the difference observed in the δ peak width and shape shown in Fig. 5A occurred due to a selective interaction between the acyl chains of the CER NS with FFA C24, indicating they were in a similar position in the unit cell of the LPP. However, when measured against the maximum splitting value, as determined in a fully deuterated chain dFFA sample

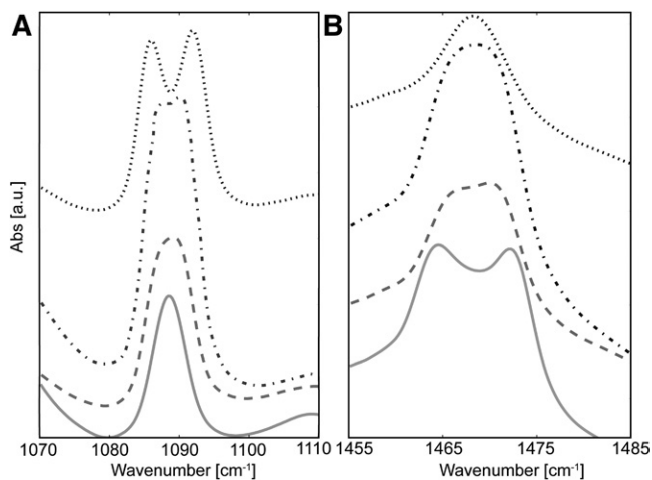


Fig. 5. FTIR peak splitting of the LPP samples at a composition of CER (EOS/NS; 0.4:0.6)/CHOL/FFA in a molar ratio of 1:1:1 at the CD_2 δ vibrational energy (A) and CH_2 δ vibration energy (B) for when the CER NS was deuterated [LPP-dNS (—)], the FFAs were deuterated [LPP-dFFAs (—)], both CER NS and the FFA C24 were deuterated [LPP-dNS/dC24 (— · —)], and CER NS and all the FFA chain lengths were deuterated [LPP-dNS/dFFAs (···)]. Samples were measured when the lipids were in the orthorhombic phase at 1°C.

(7.6 nm; Fig. 6B), the splitting length remained shorter and the splitting shape was poor. This indicated that there was still protiated chains interacting with the deuterated chains. In contrast, the width and shape of the CH_2 splitting shown in Fig. 5B did not significantly change when comparing LPP-dNS/dC24 and LPP-dFFA. Both samples had the same δ CH_2 peak width (6.2 nm; Table 2) and peak shape; the lack of difference between these samples implies that a similar number of CH_2 - CH_2 and CH_2 - CD_2 interactions were present at the same extent in each of these samples.

CD_2 peak splitting for LPP-dNS/dFFA was well-defined, with a deep minima, indicating a drastic reduction of CD_2 - CH_2 interactions compared with that observed in the other LPP samples. In addition, the splitting value was the closest to the maximum CD_2 peak splitting measured (6.6 and 7.6 nm, respectively; Table 2). In combination with the deep minima between the split peak, a reduction in the CD_2 - CH_2 interactions was observed. The deeper minima between the split peaks arose from the deuterated CER NS acyl chains and the deuterated FFAs, including the shorter chains, interacting with one another.

The LPP-dNS/dFFAs sample's CH_2 interactions included the CER EOS, CHOL, and CER NS chain, which formed a single broad peak (Fig. 5B). CHOL was incapable of interacting with neighboring alkyl chains in an equivalent

TABLE 2. δ Splitting values for CD_2 and CH_2 vibrations at 1°C

Sample	CD_2 Splitting Width (cm^{-1})	CH_2 Splitting Width (cm^{-1})
dFFA	7.6	—
LB-dNS/dFFA	7.6	—
LB-dNS/dC24	0	—
LPP- CH_2	—	10.8
LPP-dNS/dFFAs	6.6	—
LPP-dNS/dC24	4.6	6.2
LPP-dFFAs	3.8	6.2
LPP-dNS	—	9.1

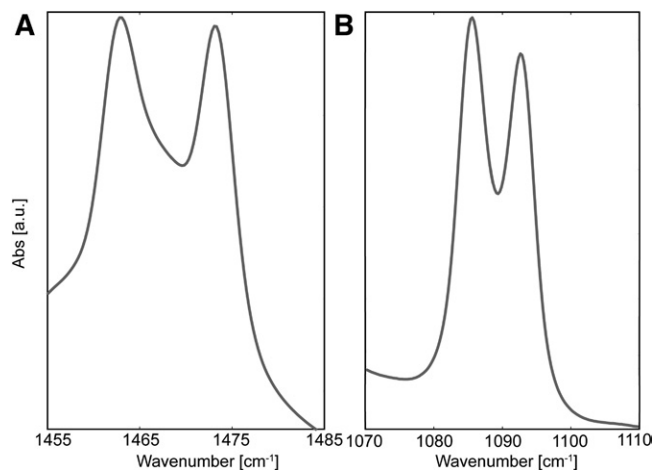


Fig. 6. Maximum peak splitting of the δ vibration. A: To measure the maximum CH_2 δ splitting, the fully protiated LPP- CH_2 samples were measured, with a peak splitting value of 10.8 cm^{-1} . B: The CD_2 maxima vibrations were measured as 7.6 cm^{-1} using the fully deuterated dFFA sample. Samples were measured when the lipids were in the orthorhombic phase at 1°C.

manner as the other lipids in the LPP due to its short-branched alkyl chain. The single broad CH_2 peak implies that some CH_2 interactions between the CER EOS and CER NS was experienced; however, due to the absence of peak splitting, no large protiated domains consisting of only CER EOS and CER NS chains were present.

Spitting effects due to CER NS protiated chain

Removing all of the fully protiated molecules from the partially deuterated LPP samples left only CER NS and FFAs, which were mixed at the same molar ratios found in the LPP-dNS/dC24 and LPP-dNS/dFFAs samples (6:4 and 3:5, respectively). The only protiated chains in these samples were the sphingosine groups of the CER NS and thus resulted in much higher CD_2 concentrations in the LB compared with the LPP samples. SAXD analysis identified the formation of one or two lamellar structures of various repeat distances in each of the samples, evident by the multiple peaks that were present at $q = 1 - 1.5\text{ nm}^{-1}$ (S2). The ν vibrations of the LB samples (S3) showed that both the CD_2 and CH_2 chains melted at the same temperature, showing that the lipids were mixed together while forming multiple lamellar structures.

In the LB-dNS/dC24 sample the CD_2 δ peak did not split (Fig. 7A); instead, a single sharp peak was observed, implying a limited number of CD_2 - CD_2 interactions. In contrast, when the FFA content was increased in the LB-dNS/dFFA sample, a split of 7.6 cm^{-1} was measured (Fig. 7A, Table 2), which matched the maximum splitting width measured in the dFFA sample. However, the minima between the split peaks was much shallower for the LB-dNS/dFFA sample compared with the fully deuterated dFFA and LPP-dNS/dFFA samples, indicating a larger number of CH_2 - CD_2 interactions. Conversely, the CH_2 δ peak did not split, but a broad peak was observed for both LB-dNS/dC24 and LB-dNS/dFFA despite the large difference in the CER-FFA ratio between these samples (Fig. 7B). As a result, within

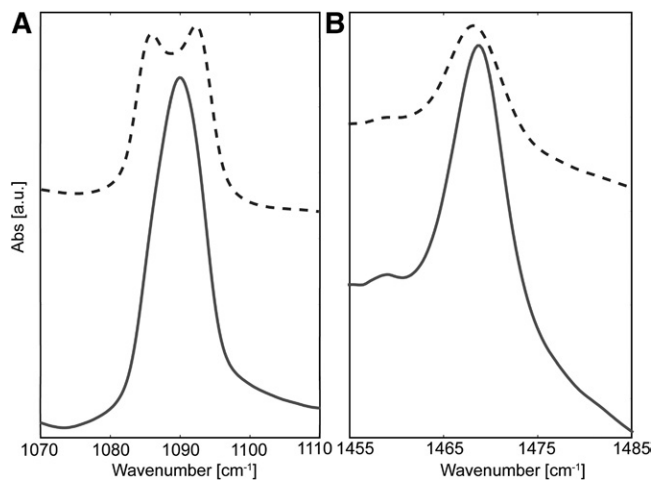


Fig. 7. Peak splitting of LB samples at a composition of CER NS and FFA at the CD_2 δ vibrational energy (A) and CH_2 δ vibration energy (B) for LB-dNS/dC24 (6:4) (—) and LB-dNS/dFFA (3:5) (---). Samples were measured when the lipids were in the orthorhombic phase at 1°C .

the LB structure, it seems that the CER sphingosine chains did not aggregate together but were dispersed between the perdeuterated chains.

DISCUSSION

In this study, the use of FTIR enabled the identification of alkyl chain interactions and domain size between equivalent isotopic chains in the orthorhombic phase (23). Based on the extended splitting and deep minima between the split peaks of the CD_2 δ vibrations, the results indicate that the CER NS acyl chains and FFAs preferentially mixed with one another in the LPP phase. By comparing the CD_2 δ vibrations of the LPP-dNS/dC24 with the LPP-dNS/dFFA, we identified that a range of FFA chain lengths were present in the central region of the LPP.

The use of simple model systems

Model systems are ideal samples for investigating various aspects of the SC, including the contribution of lipid subclasses and structural information. A wide array of models have been developed that can mimic the SC of native skin. Combining isolated CERs, CHOL, and FFAs, the structures in the SC of native skin can be accurately reproduced (26, 27). Additional studies with synthetic CERs mimicking the pig CER composition have revealed a very similar phase behavior (28, 29). We recently showed that with only CER EOS (linoleate-esterified ω -hydroxyl C30 acyl chain linked to a C18 NS) and CER NS (nonhydroxy C24 acyl chain linked to a C18 NS base) can form the LPP. The use of synthetic CERs has an additional advantage of specifically reproducing particular traits of interest for further study. One such example is when the CER composition consists of 15 mol% CER EOS and 85 mol% CER NS together with CHOL and FFA, it can mimic the phase behavior in native SC: the lipids assemble into mixed LPP/SPP with a predominant orthorhombic packing. If the concentration of

CER EOS is increased to 40 mol% of the CERs, the LPP is exclusively formed with a similar repeat distance and intensity distribution of the diffraction peaks, demonstrating the electron density distribution in the unit cell that matches the LPP in the complex systems (20, 21, 29).

The lipid models derived from synthetic CERs can range from simple models containing the minimal number of lipid subclasses to highly complex models containing many different lipid subclasses. These models can reproduce different aspects of the lipid organization, including the lamellar phase [SPP (30) or LPP (17, 18)] and lateral packing [orthorhombic or hexagonal phase (31–34)], or mimic the lipid matrix barrier capabilities against a particular drug model compared with native SC (35–37). These simpler models can simultaneously provide unambiguous information on the interactions between lipid-specific subclasses. In consideration of the similarities between isolated and simple CER compositions, in terms of the structure and properties, lipid models can offer many advantages when studying the SC lipid matrix.

Arrangement of the lipids in the LPP Model

Mojumdar et al. (17, 18) have previously identified the location of deuterated components within a synthetic LPP unit lattice to construct a molecular model (S1). In this model, the CER NS fatty acid chains, CER EOS linoleic acid and FFA C24, were identified to reside in the center of the LPP unit cell, while CHOL and a small fraction of the FFA C24 and CER NS acyl chain was also present in the outer regions of the LPP. However, no indication of the lipid chain organization within their respective regions (mixed or separate domains) was reported. In this study we focused on the localization of FFAs and CER NS to identify the lipid organization. **Table 3** shows the CH_2 - CD_2 ratio of the LPP and LB samples. The bulky short alkyl chains of CHOL cannot interact with the neighboring lipids because of the longer linear chains of the other lipids; thus, any potential CHOL alkyl chain contributions were excluded from the CH_2 total. If the lipids were distributed randomly in both the LPP and LB systems, then the same large number of CD_2 - CH_2 interactions and a smaller number of CH_2 - CH_2 interactions would be expected in both of these systems. However, the LPP δ CD_2 peak splitting was deeper and more defined compared with their LB sample counterparts despite the much higher CH_2 - CD_2 group ratio in the LPP sample. This indicates that the FFAs and the acyl chain of CER NS within the LPP colocalized with one another. Therefore, these results correlate with the LPP structure identified by Mojumdar et al. (18), where the CER NS and FFA are positioned primarily together in the central layer in the LPP unit cell.

TABLE 3. CH_2/CD_2 group ratio when CER NS and FFAs were deuterated in the LPP and LB samples

Sample	CH_2/CD_2 Ratio
LPP-dNS/dC24	2.20
LPP-dNS/dFFAs	1.07
LB-dNS/dC24	0.39
LB-dNS/dFFA	0.28

Conformation of CER NS

The conformation of the double-chained CERs remains uncertain in model systems. CERs in a membrane can either be arranged in an extended conformation, with the chains pointing in opposite directions, or as a hairpin, with the chains pointing in the same direction (Fig. 1). In the LB system the bilayer is repeatedly symmetric; thus, the CER NS experiences the same environment regardless of its arrangement. Due to the similarity of the environment, no change in the δ peak splitting would be observed for either conformation. In contrast, the CER NS chain in the trilayer LPP would experience different local environments depending on its conformation. In the LPP structure, FFAs and the acyl chain of CER NS are concentrated in the central layer, while CHOL and CER EOS are concentrated in the two outer layers. If CER NS had adopted a hairpin structure, the protiated NS alkyl chain would be in the deuterated-rich center, increasing the $\text{CD}_2\text{-CH}_2$ interactions. In contrast, if extended, the protiated NS alkyl chain would be in the hydrogen-rich outer regions, and a reduction in the number of $\text{CD}_2\text{-CH}_2$ interactions would be expected.

The CD_2 δ peak splitting in the LPP-dNS/dC24 and LPP-dNS/dFFA samples were more defined, with deeper minima points between the peaks, compared with their LB counterparts. The greater δ peak splitting in the LPP samples implied that fewer mixed $\text{CD}_2\text{-CH}_2$ interactions and more $\text{CD}_2\text{-CD}_2$ interactions were present despite the higher $\text{CH}_2\text{-CD}_2$ molar ratio. The reduced $\text{CH}_2\text{-CD}_2$ and increased $\text{CD}_2\text{-CD}_2$ interactions indicates that most of the protiated NS chains were arranged out of the way of the deuterated chains, which could only be accommodated if the CER NS had arranged into an extended conformation.


Extended CERs are known to offer several advantages to the SC over the hairpin structure, including smaller polar head group cross-sections, reduced packing strain, and connecting adjacent lamellae, thus reducing permeable boundaries (38). The smaller polar head group cross-section would enable a greater packing density, which would encourage the barrier function (39, 40). The connection between lamellae layers would discourage swelling, even in the more fluid region in the center of the unit cell associated with the linoleate chain (21), hence further promoting the barrier function. An additional advantage of the linear structure would be the improved adaptability of the unit cell. The typical length of the LPP is ~ 13 nm; however, due to the flexible necessity of the skin, the length may need to be able to temporarily accommodate slight differences in length. When in an extended conformation, the lipids can adjust the total length by adjusting the lipid angle along the basal plane of the lamellar phase. Angled linear CER conformations have been proposed for CER nonhydroxy phytosphingosine (41, 42) and α -hydroxy phytosphingosine (43).

Previous FTIR studies have investigated the conformation of CER NS in an SPP (5.2–5.4 nm) consisting of a CER NS (C24)/CHOL/FFA mixture, of which the CER NS was in an extended conformation. The proposed model implied that the lipids were not randomly mixed between the bilayers (44). Techniques such as ruthenium tetroxide-stained and cryo electron microscopy have not been able to

definitively determine the conformation of the CERs within mammalian SC. The lipids have been observed to adopt an extended conformation between both the internal and external layers, connecting individual layers together (45,46). In addition, the lipids have also been reported to adopt the hairpin conformation (47). Previous simulation studies have attempted to model the CER behavior in the SC; however, these studies were limited by the system size and simulation time (48). The lipid conformation is not necessarily fixed; the chains can be rearranged via a chain-flip transition (49). The activation energy of this process is low enough to validate the presence of both or either conformations in the LPP regardless of the initial conformation. The energy requirement for a chain-flip transition is approximately half of a flip-flop transition (49); the activation energy for a simulated flexible lipid bilayer for a flip-flop was calculated to be 15 kJ/mol (50).

FFA distribution

The distribution of the FFAs in the LPP is of interest in understanding the stability of the LPP structure. The wider splitting of the δ peaks of LPP-dNS/dFFA compared with LPP-dNS/dC24 illustrates that the deuterated domain size increased, which would have only occurred if the shorter FFAs were also present in the central region. These observations concur with the current theory, which states that FFAs increase the lipid density within the LPP by accommodating the different CER and CHOL structures into a single orthorhombic packed phase (51, 52) and thus would be assumed to be distributed throughout the LPP unit cell. Instead, the small amount of splitting length that is lost with the LPP-dNS/dFFA sample compared with a fully deuterated acyl chained sample (dFFA) can be attributed to two main factors: the presence of the protiated CER EOS's terminal linoleic acid in the central region (18) and isolated deuterated lipids in the outer layers of the LPP unit cell (18). In contrast, the single CH_2 δ peak, which measures the interactions primarily in the outer region, may not split due to the CHOL disrupting possible CH_2 interactions between CER EOS and CER NS chains.

In this study using FTIR and SAXD, we examined the local environment of the lipid alkyl chains within a simple LPP and LB model by selectively deuterating the lipid acyl chains and studying their local isotopic environment. The arrangement of these lipids were identified by the split peak properties when in the orthorhombic phase. The results revealed that the CER NS acyl chain and the FFAs are colocalized with one another within the central region of the LPP, correlating with previous models. In addition, when in the center, the CER NS adopted an extended conformation, removing the NS chain from the central region of the LPP. This extended arrangement of the CERs can potentially offer several advantages to the barrier function, facilitating 1) increased packing density, 2) inhibiting swelling, and 3) enabling flexibility in the system. This information would be beneficial in the future to examine the molecular localization of other molecules in the unit cell and to provide more insight into their interactions. 

The authors thank Evonik (Essen, Germany) for their kind contribution of deuterated CERs and the personnel at the BM26 Dutch-Belgian beamline at the European Synchrotron Radiation Facility (Grenoble, France) for their assistance during the X-ray diffraction measurements.

REFERENCES

1. Michaels, A. S., S. K. Chandrasekaran, and J. E. Shaw. 1975. Drug permeation through human skin: theory and in vitro experimental measurement. *AICHE J.* **21**: 985–996.
2. Janssens, M., J. van Smeden, G. S. Gooris, W. Bras, G. Portale, P. J. Caspers, R. J. Vreeken, T. Hankemeier, S. Kezic, R. Wolterbeek, et al. 2012. Increase in short-chain ceramides correlates with an altered lipid organization and decreased barrier function in atopic eczema patients. *J. Lipid Res.* **53**: 2755–2766.
3. Janssens, M., J. van Smeden, G. S. Gooris, W. Bras, G. Portale, P. J. Caspers, R. J. Vreeken, S. Kezic, A. P. M. Lavrijsen, and J. A. Bouwstra. 2011. Lamellar lipid organization and ceramide composition in the stratum corneum of patients with atopic eczema. *J. Invest. Dermatol.* **131**: 2136–2138.
4. van Smeden, J., M. Janssens, E. C. J. Kaye, P. J. Caspers, A. P. Lavrijsen, R. J. Vreeken, and J. A. Bouwstra. 2014. The importance of free fatty acid chain length for the skin barrier function in atopic eczema patients. *Exp. Dermatol.* **23**: 45–52.
5. van Smeden, J., M. Janssens, G. S. Gooris, and J. A. Bouwstra. 2014. The important role of stratum corneum lipids for the cutaneous barrier function. *Biochim. Biophys. Acta.* **1841**: 295–313.
6. Ishikawa, J., H. Narita, N. Kondo, M. Hotta, Y. Takagi, Y. Masukawa, T. Kitahara, Y. Takema, S. Koyano, S. Yamazaki, et al. 2010. Changes in the ceramide profile of atopic dermatitis patients. *J. Invest. Dermatol.* **130**: 2511–2514.
7. Di Nardo, A., P. Wertz, A. Gianneti, and S. Seidenari. 1998. Ceramide and cholesterol composition of the skin of patients with atopic dermatitis. *Acta Derm. Venereol.* **78**: 27–30.
8. Boiten, W. A., T. Berkers, S. Absalah, J. van Smeden, A. P. M. Lavrijsen, and J. A. Bouwstra. 2018. Applying a vernix caseosa based formulation accelerates skin barrier repair by modulating lipid biosynthesis. *J. Lipid Res.* **59**: 250–260.
9. Weerheim, A., and M. Ponc. 2001. Determination of stratum corneum lipid profile by tape stripping in combination with high-performance thin-layer chromatography. *Arch. Dermatol. Res.* **293**: 191–199.
10. van Smeden, J., and J. A. Bouwstra. 2016. Stratum corneum lipids: their role for the skin barrier function in healthy subjects and atopic dermatitis patients. *Curr. Probl. Dermatol.* **49**: 8–26.
11. Wertz, P. W., and D. T. Downing. 1991. Epidermal lipids. In *Physiology, Biochemistry and Molecular Biology of the Skin*. L. A. Goldsmith, editor. Oxford University Press, Oxford, UK. 205–235.
12. Wertz, P. W., M. Kremer, and C. A. Squier. 1992. Comparison of lipids from epidermal and palatal stratum corneum. *J. Invest. Dermatol.* **98**: 375–378.
13. Norlén, L., I. Nicander, A. Lundsjö, T. Cronholm, and B. Forslind. 1998. A new HPLC-based method for the quantitative analysis of inner stratum corneum lipids with special reference to the free fatty acid fraction. *Arch. Dermatol. Res.* **290**: 508–516.
14. Bouwstra, J. A., G. S. Gooris, J. A. van der Spek, and W. Bras. 1991. Structural investigations of human stratum corneum by small-angle X-ray scattering. *J. Invest. Dermatol.* **97**: 1005–1012.
15. Bouwstra, J., G. Gooris, and M. Ponc. 2002. The lipid organisation of the skin barrier: liquid and crystalline domains coexist in lamellar phases. *J. Biol. Phys.* **28**: 211–223.
16. de Jager, M. W., M. P. Ponc, and J. A. Bouwstra. 2011. The lipid organisation in stratum corneum and model systems based on ceramides. In *Enhancement in Drug Delivery*. E. Touitou and B. W. Barry, editors. CRC Press, Boca Raton, FL. Chapter 11. 217–232.
17. Mojumdar, E. H., G. S. Gooris, D. J. Barlow, M. J. Lawrence, B. Deme, and J. A. Bouwstra. 2015. Skin lipids: localization of ceramide and fatty acid in the unit cell of the long periodicity phase. *Biophys. J.* **108**: 2670–2679.
18. Mojumdar, E. H., G. S. Gooris, D. Groen, D. J. Barlow, M. J. Lawrence, B. Demé, and J. A. Bouwstra. 2016. Stratum corneum lipid matrix: location of acyl ceramide and cholesterol in the unit cell of the long periodicity phase. *Biochim. Biophys. Acta.* **1858**: 1926–1934.
19. Eichner, A., S. Sonnenberger, B. Dobner, T. Hauß, A. Schroeter, and R. H. H. Neubert. 2016. Localization of methyl-branched ceramide [EOS] species within the long-periodicity phase in stratum corneum lipid model membranes: a neutron diffraction study. *Biochim. Biophys. Acta.* **1858**: 2911–2922.
20. Gooris, G. S., M. Kamran, A. Kros, D. J. Moore, and J. A. Bouwstra. 2018. Interactions of dipalmitoylphosphatidylcholine with ceramide-based mixtures. *Biochim. Biophys. Acta.* **1860**: 1272–1281.
21. Paz Ramos, A., G. Gooris, J. Bouwstra, and M. Lafleur. 2018. Evidence of hydrocarbon nanodrops in highly ordered stratum corneum model membranes. *J. Lipid Res.* **59**: 137–143.
22. Snyder, R. G. 1961. Vibrational spectra of crystalline n-paraffins: II. Intermolecular effects. *J. Mol. Spectrosc.* **7**: 116–144.
23. Snyder, R. G., M. C. Goh, V. J. P. Srivatsavoy, H. L. Strauss, and D. L. Dorset. 1992. Measurement of the growth kinetics of microdomains in binary n-alkane solid solutions by infrared spectroscopy. *J. Phys. Chem.* **96**: 10008–10019.
24. Mendelsohn, R., E. Rabie, R. M. Walters, and C. R. Flach. 2015. Fatty acid chain length dependence of phase separation kinetics in stratum corneum models by IR spectroscopy. *J. Phys. Chem. B.* **119**: 9740–9750.
25. Snyder, R. G., H. L. Strauss, and D. A. Cates. 1995. Detection and measurement of microaggregation in binary mixtures of esters and of phospholipid dispersions. *J. Phys. Chem.* **99**: 8432–8439.
26. Bouwstra, J. A., G. S. Gooris, F. E. R. Dubelaar, and M. Ponc. 2001. Phase behavior of lipid mixtures based on human ceramides: coexistence of crystalline and liquid phases. *J. Lipid Res.* **42**: 1759–1770.
27. Bouwstra, J. A., G. S. Gooris, K. Cheng, A. Weerheim, W. Bras, and M. Ponc. 1996. Phase behavior of isolated skin lipids. *J. Lipid Res.* **37**: 999–1011.
28. de Jager, M. W., G. S. Gooris, I. P. Dolbnya, M. Ponc, and J. A. Bouwstra. 2004. Modelling the stratum corneum lipid organisation with synthetic lipid mixtures: the importance of synthetic ceramide composition. *Biochim. Biophys. Acta.* **1664**: 132–140.
29. Groen, D., G. S. Gooris, and J. A. Bouwstra. 2009. New insights into the stratum corneum lipid organization by X-ray diffraction analysis. *Biophys. J.* **97**: 2242–2249.
30. Mojumdar, E. H., D. Groen, G. S. Gooris, D. J. Barlow, M. J. Lawrence, B. Deme, and J. A. Bouwstra. 2013. Localization of cholesterol and fatty acid in a model lipid membrane: a neutron diffraction approach. *Biophys. J.* **105**: 911–918.
31. Janssens, M., G. S. Gooris, and J. A. Bouwstra. 2009. Infrared spectroscopy studies of mixtures prepared with synthetic ceramides varying in head group architecture: coexistence of liquid and crystalline phases. *Biochim. Biophys. Acta.* **1788**: 732–742.
32. Rerek, M. E., D. Van Wyck, R. Mendelsohn, and D. J. Moore. 2005. FTIR spectroscopic studies of lipid dynamics in phytosphingosine ceramide models of the stratum corneum lipid matrix. *Chem. Phys. Lipids.* **134**: 51–58.
33. Moore, D. J., M. E. Rerek, and R. Mendelsohn. 1999. Role of ceramides 2 and 5 in the structure of the stratum corneum lipid barrier. *Int. J. Cosmet. Sci.* **21**: 353–368.
34. Moore, D. J., M. E. Rerek, and R. Mendelsohn. 1997. FTIR spectroscopy studies of the conformational order and phase behavior of ceramides. *J. Phys. Chem. B.* **101**: 8933–8940.
35. de Jager, M., W. Groeninck, R. Bielsa i Guivernau, E. Andersson, N. Angelova, M. Ponc, and J. Bouwstra. 2006. A novel in vitro percutaneous penetration model: evaluation of barrier properties with p-aminobenzoic acid and two of its derivatives. *Pharm. Res.* **23**: 951–960.
36. Skolová, B., B. Janušová, J. Zbytovská, G. Gooris, J. Bouwstra, P. Slepíčka, P. Berka, J. Roh, K. Palát, A. Hrabálek, et al. 2013. Ceramides in the skin lipid membranes: length matters. *Langmuir.* **29**: 15624–15633.
37. Janušová, B., J. Zbytovská, P. Lorenc, H. Vavryšová, K. Palát, A. Hrabálek, and K. Vávrová. 2011. Effect of ceramide acyl chain length on skin permeability and thermotropic phase behavior of model stratum corneum lipid membranes. *Biochim. Biophys. Acta.* **1811**: 129–137.
38. Vávrová, K., A. Kováčik, and L. Opálka. 2017. Ceramides in the skin barrier. *Eur. Pharm. J.* **64**: 28–35.
39. Mojumdar, E. H., R. W. J. Helder, G. S. Gooris, and J. A. Bouwstra. 2014. Monounsaturated fatty acids reduce the barrier of stratum corneum lipid membranes by enhancing the formation of a hexagonal lateral packing. *Langmuir.* **30**: 6534–6543.
40. Skolová, B., A. Kováčik, O. Tesař, L. Opálka, and K. Vávrová. 2017. Phytosphingosine, sphingosine and dihydrosphingosine ceramides in

- model skin lipid membranes: permeability and biophysics. *Biochim. Biophys. Acta*. **1859**: 824–834.
41. Raudenkolb, S., W. Hübner, W. Rettig, S. Wartewig, and R. H. H. Neubert. 2003. Polymorphism of Ceramide 3. Part I: an investigation focused on the head group of N-octadecanoylphyto sphingosine. *Chem. Phys. Lipids*. **123**: 9–17.
 42. Wartewig, S., and R. H. H. Neubert. 2007. Properties of ceramides and their impact on the stratum corneum structure: a review. *Skin Pharmacol. Physiol*. **20**: 220–229.
 43. Raudenkolb, S., S. Wartewig, and R. H. H. Neubert. 2005. Polymorphism of ceramide 6: a vibrational spectroscopic and X-ray powder diffraction investigation of the diastereomers of N-(α -hydroxyoctadecanoyl)-phyto sphingosine. *Chem. Phys. Lipids*. **133**: 89–102.
 44. Školová, B., K. Hudská, P. Pullmannová, A. Kováčik, K. Palát, J. Roh, J. Fleddermann, I. Estrela-Lopis, and K. Vávrová. 2014. Different phase behavior and packing of ceramides with long (C16) and very long (C24) acyls in model membranes: infrared spectroscopy using deuterated lipids. *J. Phys. Chem. B*. **118**: 10460–10470.
 45. Iwai, I., H. Han, L. d. Hollander, S. Svensson, L-G. Öfverstedt, J. Anwar, J. Brewer, M. Bloksgaard, A. Laloef, D. Nosek, et al. 2012. The human skin barrier is organized as stacked bilayers of fully extended ceramides with cholesterol molecules associated with the ceramide sphingoid moiety. *J. Invest. Dermatol*. **132**: 2215–2225.
 46. Swartzendruber, D. C., P. W. Wertz, D. J. Kitko, K. C. Madison, and D. T. Downing. 1989. Molecular models of the intercellular lipid lamellae in mammalian stratum corneum. *J. Invest. Dermatol*. **92**: 251–257.
 47. Kuempel, D., D. C. Swartzendruber, C. A. Squier, and P. W. Wertz. 1998. In vitro reconstitution of stratum corneum lipid lamellae. *Biochim. Biophys. Acta*. **1372**: 135–140.
 48. Das, C., and P. D. Olmsted. 2016. The physics of stratum corneum lipid membranes. *Philos Trans A Math Phys Eng Sci*. **374**: 20150126.
 49. Kiselev, M. A. 2007. Conformation of ceramide 6 molecules and chain-flip transitions in the lipid matrix of the outermost layer of mammalian skin, the stratum corneum. *Crystallogr. Rep*. **52**: 525–528.
 50. Marti, J., and F. Csajka. 2003. Flip-flop dynamics in a model lipid bilayer membrane. *Europhys. Lett*. **61**: 409–414.
 51. Bouwstra, J. A., G. S. Gooris, F. E. R. Dubbelaar, M. Ponc, and A. M. Weerheim. 1998. pH, cholesterol sulfate, and fatty acids affect the stratum corneum lipid organization. *J. Investig. Dermatol. Symp. Proc*. **3**: 69–74.
 52. Bouwstra, J., F. Dubbelaar, G. Gooris, and M. Ponc. 2000. The lipid organisation in the skin barrier. *Acta Dermato Venereologica Suppl. (Stockh.)*. **208**: 23–30.